

# Lab on a Chip

Accepted Manuscript

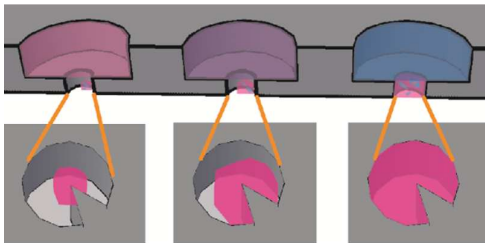


This is an *Accepted Manuscript*, which has been through the Royal Society of Chemistry peer review process and has been accepted for publication.

*Accepted Manuscripts* are published online shortly after acceptance, before technical editing, formatting and proof reading. Using this free service, authors can make their results available to the community, in citable form, before we publish the edited article. We will replace this *Accepted Manuscript* with the edited and formatted *Advance Article* as soon as it is available.

You can find more information about *Accepted Manuscripts* in the [Information for Authors](#).

Please note that technical editing may introduce minor changes to the text and/or graphics, which may alter content. The journal's standard [Terms & Conditions](#) and the [Ethical guidelines](#) still apply. In no event shall the Royal Society of Chemistry be held responsible for any errors or omissions in this *Accepted Manuscript* or any consequences arising from the use of any information it contains.



Label free biomechanical readout for high-throughput phenotypic drug screening is achieved on bi-Content Contractility-based micro-Collagen Chip (3CChip)

## Bi-content micro-collagen chip provides contractility-based biomechanical readout for phenotypic drug screening with expanded and profiled targets

Hui Zhao<sup>ab‡</sup>, Lyu Zhou<sup>ab‡</sup>, Qiang Zhang<sup>c</sup>, Xiaoying Zhou<sup>d</sup>, Yonghui Zhang<sup>d</sup>, Huijun Chen<sup>c</sup>, Yanan Du<sup>\*b</sup>

<sup>a</sup> School of Life Sciences, Tsinghua University, Beijing, 10084, China

<sup>b</sup> Department of Biomedical Engineering, School of Medicine, Collaborative Innovation Center for Diagnosis and Treatment of Infectious Disease, Tsinghua University, Beijing, 10084, China. Email: duyanan@tsinghua.edu.cn; Tel.: +86-10-62781691; Fax: +86-10-62773380

<sup>c</sup> Center for Biomedical Imaging Research, Department of Biomedical Engineering, School of Medicine, Tsinghua University, Beijing, 10084, China

<sup>d</sup> Department of Pharmacology and Pharmaceutical Sciences, School of Medicine, Tsinghua University, Beijing, 10084, China

‡ These authors contributed equally to this work.

**Abstract**

Phenotypic screening regains new momentum in pharmaceutical industry owing to its exceeded success over target-based screenings. Most phenotypic screenings rely on nonspecific biochemical readout regarding cellular viability which hampers the discovery of novel druggable mechanism of actions (MOAs). Here we present Contractility-based bi-Content micro-Collagen Chip (3CChip), which innovates cellular contractility as a biomechanics-related phenotype for drug screening. Bi-content analysis on cell contractility (imaged by iPhone) and viability suggests that the label-free contractility-based analysis exhibits superior sensitivity to compounds targeting contractile elements (*e.g.* focal adhesion, cytoskeleton), resulting in enlarged target pool for drug assessment. Six typical readout patterns of drug response are summarized according to relative positions of contraction/viability curves and drug targets are profiled into three categories (biomechanical, biochemical and house-keeping) by 3CChip, which would benefit subsequent target identification. The simple-to-use and effective 3CChip offers a robust platform for micro-tissue-based functional screening and may lead to a new era of mechanism-informed phenotypic drug discovery.

**Keywords:** phenotypic drug screening; micro-collagen contraction; cellular contractility; biomechanical readout; drug target profiling

## 1. Introduction

Phenotypic screening as an original drug discovery paradigm has gained extensive success in drug development in the past decades and is currently attracting resurgence of interest in pharmaceutical industry.<sup>1</sup> In contrast to target based screening which usually screen against targets lack of cellular milieu (*e.g.* recombinant purified proteins), phenotypic assays provide additional biological complexity so that multiple interactive targets and signaling pathways can be synchronously involved and analyzed. However, core phenotypes used in conventional phenotypic screenings have heavily relied on cytotoxicity readouts, in particular cell viability assays, which limit the discovery of novel druggable molecular mechanism of actions (MOAs).<sup>2</sup>

Working mechanism for canonical cell viability assays is virtually based on specific metabolic enzyme activities or cell membrane permeability, as exemplified by MTT/MTS assay and ATP assay respectively. Alamar Blue assay is also among the most popular cell viability assays performed to assess compound cytotoxicity by measuring mitochondrial related reductase activity on reducing the dark blue resazurin to fluorescent resorufin.<sup>3</sup> Although assays in these categories make the bedrock of phenotypic screenings, it is evident that too much reliance on such nonspecific cellular response hampers the discovery of new therapeutically relevant targets. To establish extended linkages between target involvement, cellular effects and desired phenotypes, Moffat et al. recently proposed the concept of mechanism-informed phenotypic drug discovery (MIPDD),<sup>2</sup> represented by specific signaling pathway assays in cancer drug development. Reporter genes (*e.g.* fluorescence proteins, luciferase enzyme) producing the measurable readout (fluorescence or luminescence) are basically required in phenotypic screenings which are designed to identify active compounds that have effects on an appointed signaling pathway (*e.g.* Tumor

Necrosis Factor pathway<sup>4</sup>) or a disease-specific phenotype (*e.g.* neurite outgrowth assays for Alzheimer disease<sup>5</sup>). Despite of efforts to develop new platforms for MIPDD, output signals of current phenotypic screenings are exclusively restricted to biochemical readouts reflecting up or down regulation of particular genes or proteins.

Another intense debate on the drawback of current phenotypic drug screening approaches is that cells are routinely maintained on two-dimensional (2D) planar substrates, which are distinctly different from the *in vivo* three-dimensional (3D) microenvironment comprised of highly communicative cell-cell/cell-matrix interactions. Cells grown in 2D monolayer commonly demonstrate non-physiological features and may substantially lose therapeutically translatable multicellular phenotypes, making them poor surrogates of pathological tissues. Recent research efforts on 3D cell cultures have employed spheroids, porous scaffold or hydrogel based cell culture systems for more biomimetic cellular behaviors and drug responses.<sup>6-11</sup> Nonetheless, moving forward drug assessment from 2D to 3D is currently obstructed by the lack of convenient, scalable and consistent cell culture format. Additional limitations arise from the fact that current phenotypic readouts in 3D systems are substantially the same as their conventional 2D counterparts, which are fundamentally based on biochemical signals, for instance fluorescent or colorimetric readout obtained by Alamar Blue assay, Live/Dead staining [Calcein AM for live cells, Propidium Iodide (PI) for dead cells], or reporter gene expression related to designated signaling pathway. However, accessibility of imaging and analysis is much more difficult and less accurate in 3D systems due to disturbance from non-cellular materials or limitations in 3D light transmission. Therefore, 3D tissue-based high throughput models with reliable non-canonical phenotypic readout are in great need to realize more predictive and informative drug screening

outcomes.

In an effort to address the above-mentioned unmet challenges, we are inspired by collagen contraction assay, an old methodology firstly reported more than thirty years ago for studying wound healing or fibroblast biology.<sup>12,13</sup> Cells embedded in collagen lattices dynamically interact with collagen fibrils, reorganize and contract the matrix, resulting in shrinkage of the gel body. The contractility of cells could be estimated by quantifying the final gel area without any additional biochemical labeling processes. Furthermore, as a critical biomechanical regulator that shares molecular basis with many other cell functions (*e.g.* cell migration), cellular contractility is tightly associated with *in vivo* pathological processes such as tumour metastasis and heart failure.<sup>14</sup> Hence, given most cells have inherent capacity to contract and remodel surrounding matrix, we hypothesize that cellular contractility could be developed as a new phenotypic drug screening readout which is naturally label-free and three dimensional.

Taking advantage of advances in microfabrication and biomaterials,<sup>15</sup> here we develop Contractility-based bi-Content micro-Collagen Chip (3CChip), which outstrips traditional cell-based models with additional biomechanical readout, empowering high throughput tissue-level functional phenotypic drug screening. To the best of our knowledge, it is the first time to utilize cell contractility as a quantitative phenotypic readout for drug discovery. The miniaturizable and automated formation and operation of micro-tissues and label-free image-based readout in this platform make it extremely cost-effective and user-friendly. We anticipate that this functional micro-tissue based 3CChip will find extensive applications in pharmaceutical industry to facilitate phenotypic-based drug discovery.

## 2. Materials and methods

### 2.1. Chip fabrication

To fabricate micro-tissue laden chips, a 0.5 mm PMMA (Polymethylmethacrylate, Sunjin Electronics Co., Ltd., China) plastic plate was engraved according to the design of Supplementary Fig. 2 with the engraver Rayjet 50 (Trotec, Austria). To fabricate reservoir chips, the protective membrane of one side of a 1 mm PMMA plastic plate was removed, and a piece of 467MP adhesive (3M, MN) was stucked onto the side. The 1 mm PMMA plastic plate was engraved with adhesive according to the design of Supplementary Fig. 1 with the engraver Rayjet 50. The protective membranes of reverse sides of a micro-tissue laden chip and a reservoir chip were removed and chips were assembled.

### 2.2. Cell seeding and culture on 3CChip

Detailed procedures were shown in Supplementary Video 1. Briefly, the assembled chips were exposed under UV for over 1 h for sterilization. Rat tail high concentration collagen type I (BD Biosciences, MA) stock solution was diluted to 2 mg/ml with precooled complete medium containing 1 M NaOH and collagen stock solution at the ratio 0.023:1 (v/v). After digestion and centrifuging, the cell pellet was resuspended with collagen working solution to get cell-collagen mix of  $4 \times 10^6$  cells/ml. Cell-collagen mix was subpackaged and put on ice. 125  $\mu$ l cell-collagen mix was blended gently and immediately loaded onto the cell-laden side of an assembled chip and scraped evenly with a bent glass rod. The chips were put in a wet box at 37 °C for 1 h. After gelation, 8  $\mu$ l drug solution with gradient concentration diluted in complete medium was loaded into each reservoir. Following drugs were tested: Doxorubicin hydrochloride (Aladin, China), Y27632 (Lannuo, China), sodium azide (Amresco), Gleevec (Dalian Meilun, China), Berberine (Heowns, China), Zoledronate (AvaChem, TX), Rotenone (Sigma-Aldrich) and Simvastatin



(Heowns, China). For drugs dissolved in DMSO, 0.05% DMSO was added in complete medium as the non-drug control. Cell viability assay and contractility analysis of cardiac fibroblasts or HT-1080 were performed 30 h or 48 h later respectively.

### 2.3. On-chip Alamar Blue assay

Alamar Blue (CellTiter-Blue, Promega) stock solution was diluted 6 times with complete medium. Drug solution in the reservoirs was sucked out and each reservoir was loaded with 8  $\mu$ l Alamar Blue working solution. The chips were incubated at 37 °C for 2 h. Then fluorescence was detected from chips loaded on a self-made adaptor with a microplate reader (SpectraMax M5, Molecular Devices, CA). Excitation light was 560 nm and emission light was 590 nm. Fluorescence of non-cell control was subtracted as the background. ICV<sub>50</sub> (half maximal Inhibitory Concentration of Viability) is defined as the concentration of a certain drug that inhibits the viability of cells by half.

### 2.4. Contractility analysis

After cell viability assay, chips were washed in diH<sub>2</sub>O and soaked in 2.5% (v/v) glutaraldehyde in 0.01 M PBS (pH=7.3, 25 °C) for 15 min to fix collagen gels. Then chips were washed with diH<sub>2</sub>O and dyed for 5 min with 0.1% (m/v) ponceau S in 5% acetic acid. Chips were then washed with diH<sub>2</sub>O and photographed against a white background using iPhone 4s. To avoid deviation caused by photographing process, we fixed the whole setup including positioning of the camera and chip. Out of focus pictures were avoided also to guarantee the quality and consistency of the obtained images. The number of pixels of gels in each well was analyzed using homemade software ‘*CheckCircle.m*’ based on MATLAB (The MathWorks, Inc., MA) as referred to the manual in Supplementary Video 2.

Absolute or relative contraction was defined as follows:

Absolute contraction

= pixel number of a gel before contraction – pixel number after contraction

$$\text{Relative contraction} = \frac{\text{absolute contraction at a certain drug concentration}}{\text{absolute contraction of solvent control}}$$

ICC<sub>50</sub> (half maximal Inhibitory Concentration of Contraction) is defined as the concentration of a certain drug that inhibits the contraction function of cells by half.

### 2.5. Code availability

The code of the homemade software '*CheckCircle.m*' based on MATLAB can be accessed in Supplementary Code 1. MATLAB R2012a or later version is recommended. The code is strictly prohibited for any form of commercial purposes without written authorization.

### 2.6. Isolation of primary cardiac fibroblasts

Cardiac fibroblasts were isolated from hearts of neonatal Sprague-Dawley rats as previously described.<sup>16</sup> Briefly, 10 rat hearts were excised, rinsed with HBSS (Wisent, Canada) and cut into small pieces (1 mm<sup>3</sup>), which were then dissociated by enzymatic digestion (Collagenase type II, 100 U, Gibco, NY and 0.125% Trypsin, Wisent, Canada) at 37 °C for 10 min. The remained pieces were treated in enzyme for 5 to 6 times till no visible tissue piece could be observed. The supernatant was collected from each round and enzymes were neutralized by adding 1/10 volume of fetal bovine serum (FBS, Wisent, Canada). The liberated cells were collected by centrifugation and were resuspended in fresh medium containing 10% FBS, which were then plated in 75 cm<sup>2</sup> culture flasks. 60~80 min after plating, non-adherent cells were removed by changing medium and adherent cells (mainly fibroblasts) were further propagated for 3~4 passages. The Laboratory Animal Facility at the Tsinghua University is accredited by AAALAC (Association for Assessment and Accreditation of Laboratory Animal Care International), and all animal-related protocols in this study have

been approved by the Institutional Animal Care and Use Committee (IACUC).

### *2.7. Cell culture*

Primary cardiac fibroblasts and human fibrosarcoma cells (HT-1080, a gift from Prof. Keh Kooi Kee, School of Medicine, Tsinghua University) were cultured in high glucose Dulbecco's modified Eagle medium (4.5 g/L glucose, Wisent, Canada) with 10% FBS and 1% penicillin-streptomycin solution (Wisent, Canada) in a humidified 5% CO<sub>2</sub> incubator (Thermo) at 37 °C. Cells were subcultured and preserved according to general protocol. To study MOAs of Simvastatin and sodium azide, TGF-β1 (Cell Signaling Technology), high glucose Dulbecco's modified Eagle medium (4.5 g/L glucose, Wisent, Canada) and low glucose Dulbecco's modified Eagle medium (1 g/L glucose, Wisent, Canada) were used. For the study with or without TGF-β1, cells were cultured in high glucose medium.

### *2.8. Scanning electron microscopy*

Collagen gels with or without cells were fixed with 2.5% glutaraldehyde in deionized water for 2 h, gently washed 3 times, and then dehydrated with series of graded ethanol (30, 50, 70, 80, 90 and 100%). The samples were subsequently immersed in tert-butyl alcohol twice, each for 3 min and frozen at -20 °C. After coating with gold using a sputter coater for 60 s, cell and matrix morphology were visualized by a scanning electron microscope (SEM, FEI Quanta 200, Netherlands) at 8,000 to 20,000 magnifications.

### *2.9. Immunofluorescence staining and imaging*

Cells embedded in 3D collagen gels were fixed with 4% paraformaldehyde for 20 min at room temperature, permeabilized by 0.5% Triton X-100 for another 20 min and then blocked with 5% (w/v) bovine serum albumin (BSA, Wisent, Canada) in PBS overnight at 4 °C. Primary

antibodies, such as anti-vinculin (Abcam ab32084, diluted at 1:200), anti-paxillin (Abcam ab18058, diluted at 1:250), were incubated with samples for 12 h at 4 °C, followed by 2 h incubation with appropriate secondary antibodies (EarthOx Life Sciences, CA) at room temperature. Hoechst 33324 (Invitrogen) was used to detect nucleus. The stained samples were then observed and imaged using a Nikon confocal microscope.

For F-actin staining, the fixed and permeabilized samples were exposed to 100 nM rhodamine conjugated phalloidin for 30 min at room temperature. 0.5  $\mu$ l/ml Calcein-AM (for live cells, Wako, Japan) and 2  $\mu$ l/ml of PI (for dead cells, Wako, Japan) were incubated with samples for 15 min at 37 °C, immediately followed by microscopic imaging under Nikon Eclipse Ti-S microscope.

#### 2.10. Statistical analysis

To calculate  $IC_{50}$  values of drugs, the model of log (inhibitor) vs. response (four parameters) in GraphPad Prism 6.01 (GraphPad Software, CA) was used to fit the drug response curves. Unless specially stated, data are shown as mean $\pm$ s.d. Coefficient of variance (CV) was calculated as the ratio of s.d. to mean. Unpaired two-tail t test was used to determine statistical significance of cell numbers in the study of cell proliferation of HT-1080 on chips in Fig. 2b (n=72). Paired two-tail t test was used to determine statistical significance between  $ICV_{50}$  and  $ICC_{50}$  of a certain drug in Fig. 4l and 4r (n $\geq$ 3). Pseudo Therapeutic Index (pTI) was calculated as the ratio of  $ICV_{50}$  to  $ICC_{50}$ . Unpaired two-tail t test was used to determine statistical significance of pTI after adding TGF- $\beta$ 1 or glucose (data were obtained from two parallel chips with 6 replicate spots on each chip; s.e.m. of  $ICV_{50}$  or  $ICC_{50}$  was from fitting results of GraphPad). Symbols for statistical significance: P value $\geq$ 0.05: ns (not significant); 0.01<P value<0.05: \*, 0.001<P value<0.01: \*\*; 0.0001<P

value<0.001: \*\*\*; P value<0.0001: \*\*\*\*.

### 3. Results

#### 3.1. 3CChip fabrication and operation

The prototype of 3CChip has a two-layer structure which comprises a 96-well (3 mm in diameter and 0.5 mm in height for each well) reservoir chip on the top with a complementary micro-tissue laden chip (0.8 mm in diameter and 0.5 mm in height for each well) on the bottom (Fig. 1a,b). The two PMMA chips were separately manufactured by carbon dioxide laser ablation (Supplementary Figs 1, 2 and 3) and then assembled via highly biocompatible adhesive tapes (60  $\mu\text{m}$  in thickness) to avoid cross-contamination between adjacent wells (Supplementary Figs 4 and 5). The 3CChip were designed to have similar geometrical arrangement of the micro-wells to commercialized 384-well plates and the similar exterior dimensions to standard glass slides, making it highly compatible with existing HTS infrastructure (*e.g.* micro-plate reader, robotic handling systems). Specially, a 200  $\mu\text{m}$  hump was subtly created in each micro-well, which was expected to be an anchor for contracted gel body. As shown in Fig. 1c and Supplementary Video 1, cells mixed with collagen pre-polymer solution were scraped into the micro-tissue laden chip on the corresponding side using a bent glass rod (Supplementary Fig. 9), rapidly generating a uniform micro-tissue array ready for use upon gelation. Culture medium with appropriate drug concentration was pipetted into the top reservoir and the entire chip was then stored in a homemade (based on common tip-box) gas-permeable wet chamber preventing evaporation and ensuring long-term maintenance of the micro-scale reaction unit. Cell viability was quantified by on-chip Alamar Blue assay to obtain the ICV (Inhibition Concentration of Viability) curve (Supplementary Fig. 10). Afterwards, the 3CChip was dipped into glutaraldehyde solution for

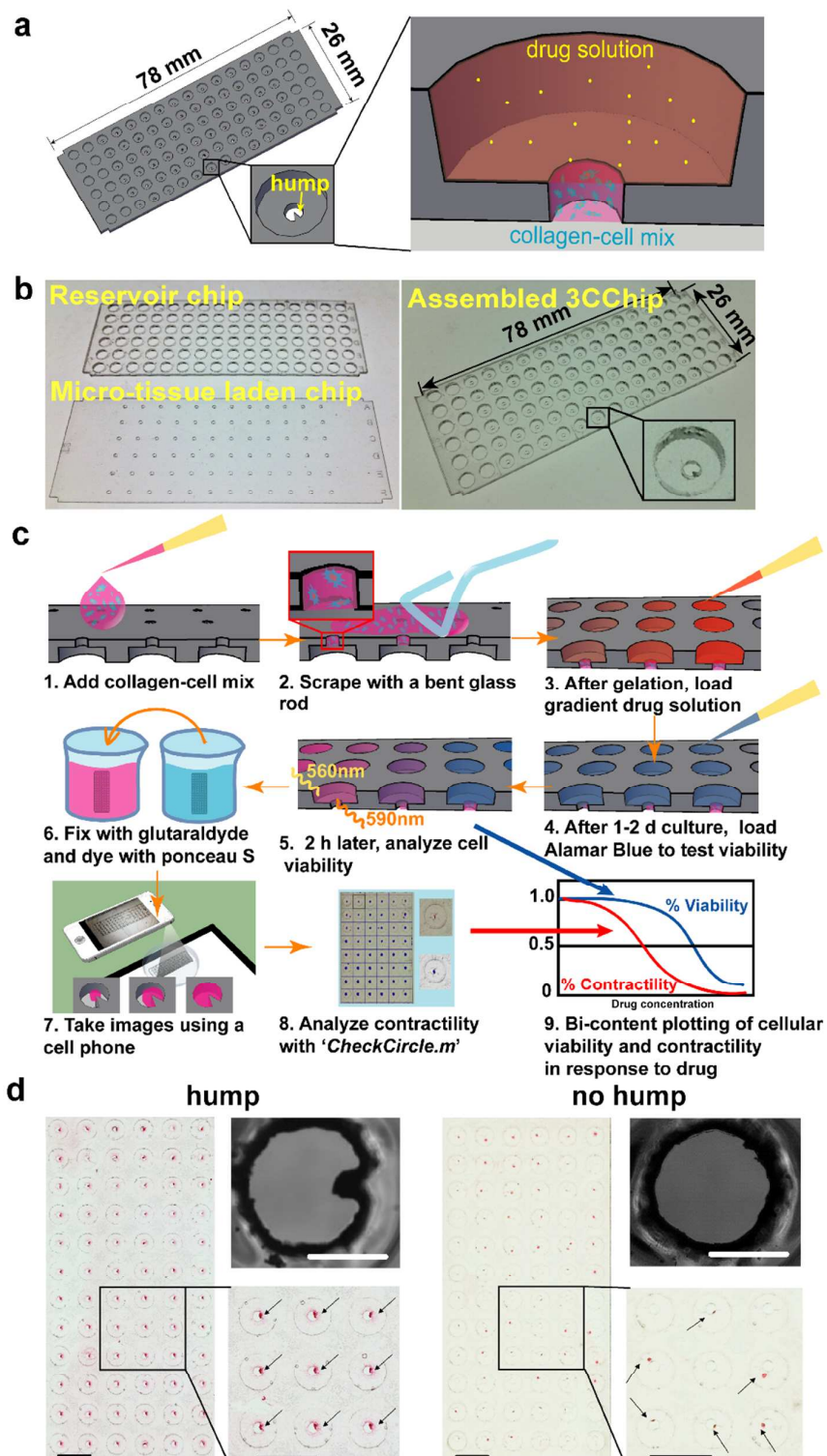


**Figure 1.** Contractility-based bi-Content micro-Collagen Chip (3CChip) for phenotypic drug screening. a) Cartoons to show the design of a 3CChip. b) Photographs of a reservoir chip and a micro-tissue laden chip with humps before and after assembly. c) Experimental procedure for 3CChip-based phenotypic drug screening. d) Comparison of micro-tissue location on chips with or without hump showing the positioning effects enabled by the hump design. Arrows indicate gel bodies. Scale bar: 5 mm (black), 500  $\mu\text{m}$  (white).

fixation of the collagen lattices in order to avoid further change of gel area during continued ponceau S dyeing. The increased contrast of gel bodies (pink in colour) against white background allowed quick and convenient imaging of the final result simply by a cell phone (*e.g.* iPhone), which has been highlighted to be the next-generation high-end imaging tool in medical practice.<sup>17</sup> MATLAB-based image analysis software '*CheckCircle.m*' (Supplementary Video 2 and Supplementary Fig. 8) was developed for data processing and the quantitative readout of ICC (Inhibition Concentration of Contraction) curve was plotted in company with the ICV curve for further analysis. Notably, the overhanging gel bodies attached to small humps in each micro-well resulting in a well-organized and homogenous gel array, compared to disorderly distributed or even lost gels in chips without hump (Fig. 1d).

### 3.2. Tissue characterization in 3CChip

Collagen solution with  $5 \times 10^5$  human fibrosarcoma cells HT-1080 was scraped on the cell-seeding side of 3CChip. Immediately upon gelation, Alamar Blue Assay was performed on 3CChip to test the homogeneity of initial cell seeding. As shown in Figure 2a ( $t=0$  h), cells distributed uniformly in the micro-wells on the entire chip [Coefficient of Variation (CV) = 0.096], with approximately 2,000 cells settled evenly in each hollow well (Supplementary Fig. 9). The estimated seeding efficiency was around 50%, explained by gel loss to the glass rod and the chip surface. The amount of cells seeded in each micro-well was controllable by altering initial scraping cell density. The concentration of collagen hydrogel was also tunable from 0.5 mg/ml to 3 mg/ml under the criteria that collagen fibers polymerized to solid 3D matrix networks. As gel contraction rate was depended on cell density and gel concentration, the exact cell number and gel concentration used for a special disease model should be optimized before drug administration



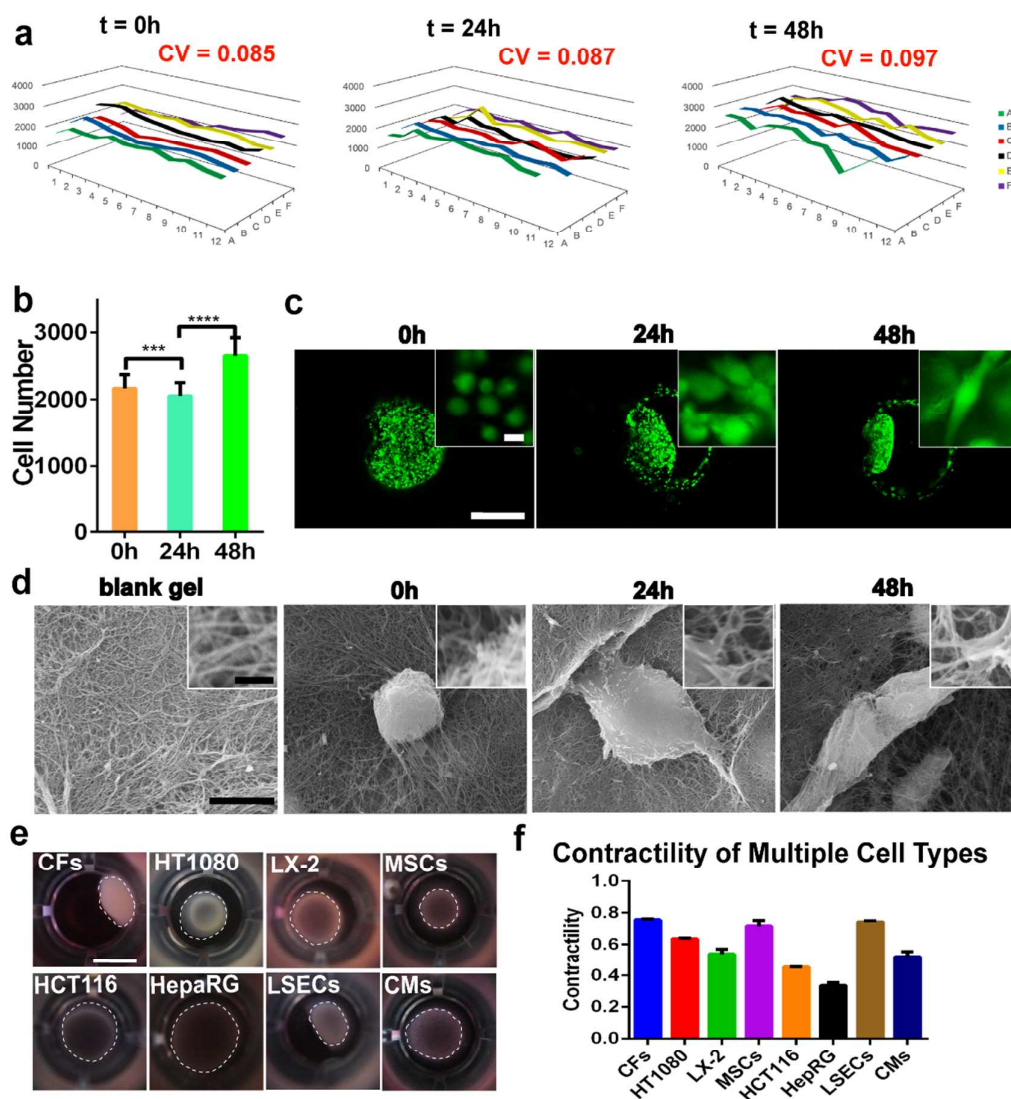


**Figure 2.** Micro-tissue cultivation and contraction on 3CChip. a) Uniform cell distribution in each well at variable time points after seeding (0 h, 24 h, 48 h) as shown by on-chip Alamar Blue assay. CV, Coefficient of Variation. b) Growth of HT-1080 cells seeded within 3CChip ( $n=72$ ). c) Change of cell morphology along with gel contraction during long term cultivation (Green: Calcein AM). Scale bar: 500  $\mu\text{m}$ . Insert scale bar: 25  $\mu\text{m}$ . d) SEM images of HT-1080 cells grown in collagen matrix showing enhanced cell matrix interactions during contraction. Scale bar: 10  $\mu\text{m}$ . Insert scale bar: 1  $\mu\text{m}$ . e) Conventional collagen contraction assay performed in 96-well plate with cells from multiple origins. Scale bar: 4 mm. f) Quantitative analysis of contractility of various cell types ( $n=3$ ). Data shown as mean $\pm$ SD  $0.0001 < P \text{ value} < 0.001$ : \*\*\*;  $P \text{ value} < 0.0001$ : \*\*\*\*.

(Supplementary Fig. 12). Cell viability was examined again after 1 or 2 days cultivation and the uniformity was still acceptable with all CV values around 0.1 (Fig. 2a,  $t=24$  h and  $t=48$  h). Slight



fluctuation was observed in cell proliferation and the slow growth rate might be owing to high initial cell seeding density (Fig. 2b). The contraction process was recorded by microscopic images at the corresponding time points, demonstrating elongated cell morphology along with contraction (Fig. 2c). To visually exhibit cell-matrix interactions in the micro-tissue, SEM images were obtained for observation of blank collagen gel matrix or cell-matrix interface (Fig. 2d). Cells extensively spread during culture with pseudopodium firmly grasping the collagen fibers, indicating strong cell-matrix interactions during contraction.

While collagen contraction assay is mostly conducted with fibroblastic cells, several studies have shown that other cell types (*e.g.* endothelial cells, epithelial cells) can also contract collagen hydrogel.<sup>18, 19</sup> Here, to demonstrate the applicability of 3CChip for cells from multiple origins, we systemically tested the contractile ability of other cell types by conventional collagen contraction assay (Fig. 2e). Both mesenchymal cells (*i.e.* primary cardiac fibroblasts, human fibrosarcoma cell line HT-1080, human hepatic stellate cell line LX-2 and mesenchymal stem cells) and non-mesenchymal cells (*i.e.* human colon cancer cells HCT16, human hepatoma cell line HepaRG, liver sinusoidal endothelial cells LSECs and primary cardiomyocytes) are capable to contract collagen matrix of given concentration (2 mg/ml). However, it should be noted that in current conditions gel contraction by HepaRG and HCT116 was not quite significant (relative contraction ratio less than 50%, Fig. 2f) compared to other cell populations, which should be further improved by varying cell or matrix density if they were applied to 3CChip.

### 3.3. Contractility-based biomechanical readout for drug assessment on 3CChip

To demonstrate the utility of 3CChip for high throughput drug screening, effects of a gold-standard anti-cancer drug doxorubicin (Dox) were examined against tumor model comprised

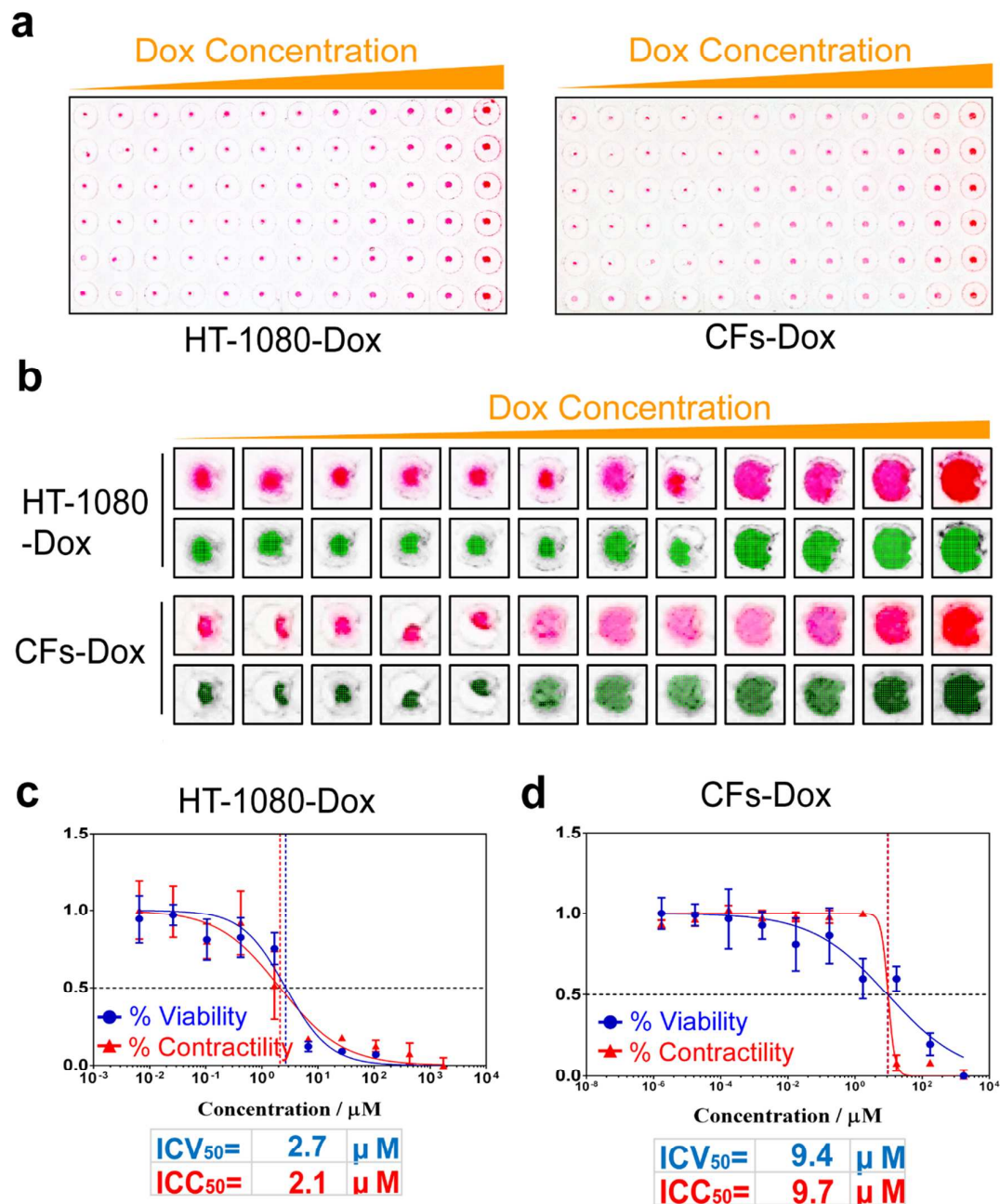


**Figure 3.** Demonstration of contractility-based biomechanical readout of drug assessment by 3CChip. a) Raw images (obtained by iPhone) of 3CChip containing micro-scale tumour (HT-1080) or fibrotic (Cardiac Fibroblasts, CFs) tissues after administration of gradient doxorubicin (Dox) for 48 h (HT-1080) or 24 h (CFs). b) Illustration of processed images using homemade software ‘CheckCircle.m’ (Pink: gel body in raw images; Green: counted pixels in processed images). c, d) Bi-content dose-response curves for Dox in tumour model (c) and fibrosis model (d). Red curves [Inhibitory Concentration of Contraction (ICC) curve] were plotted based on analysis of gel contraction images and blue curves [Inhibitory Concentration of Viability (ICV) curve] were plotted according to on-chip Alamar Blue assays. (n=6, data shown as mean±SD)

of HT-1080 cells and fibrosis model comprised of primary cardiac fibroblasts. Each concentration of Dox was administered in one column on 3CChip with six reservoirs as replicates. According to a previous study which experimentally investigated the transport dynamics of proteins like Transforming Growth Factor- $\beta$ 1 (TGF- $\beta$ 1) into collagen hydrogel,<sup>20</sup> we asserted that concentration of the diffusing small molecule drug would reach equilibrium throughout the micro-collagen gels within 30 min on 3CChip. Figure 3a showed the raw images of contracted micro-gels imaged by iPhone, which were then imported to 'CheckCircle.m' software for quantitative analysis (Fig. 3b, see Methods). The curve of contractility inhibitory effect was plotted according to normalized contraction index of different drug concentrations in parallel with relevant cell viability (Fig. 3c,d). The ICC and ICV curves tallied well with each other for Dox treated HT-1080 cells, and the ICC<sub>50</sub> (50% Inhibition Concentration of Contraction) for Dox treated CFs (9.7  $\mu$ M) also coincided with ICV<sub>50</sub> (50% Inhibition Concentration of Viability, 9.4  $\mu$ M). Interestingly, while showing analogous values of ICC<sub>50</sub> and ICV<sub>50</sub>, the overall ICC curve of CFs response to Dox showed incongruous trend with that of ICV, suggesting that drug effects might be distinctly reflected by different phenotypic readouts. These results indicate that it is possible to utilize cellular contractility as a novel biomechanical phenotypic readout for drug assessment on the easy-to-use and effective 3CChip, which is compatible for high throughput tissue-level label-free functional phenotypic screenings.

#### 3.4. Revelation of novel MOAs by 3CChip

Molecular mechanism of cellular contractility has been extensively investigated in the field of cell and molecular biology.<sup>14, 21, 22</sup> As shown in the framework in Figure 4a, molecular elements related to contractility are classified into three zones according to their roles played in the

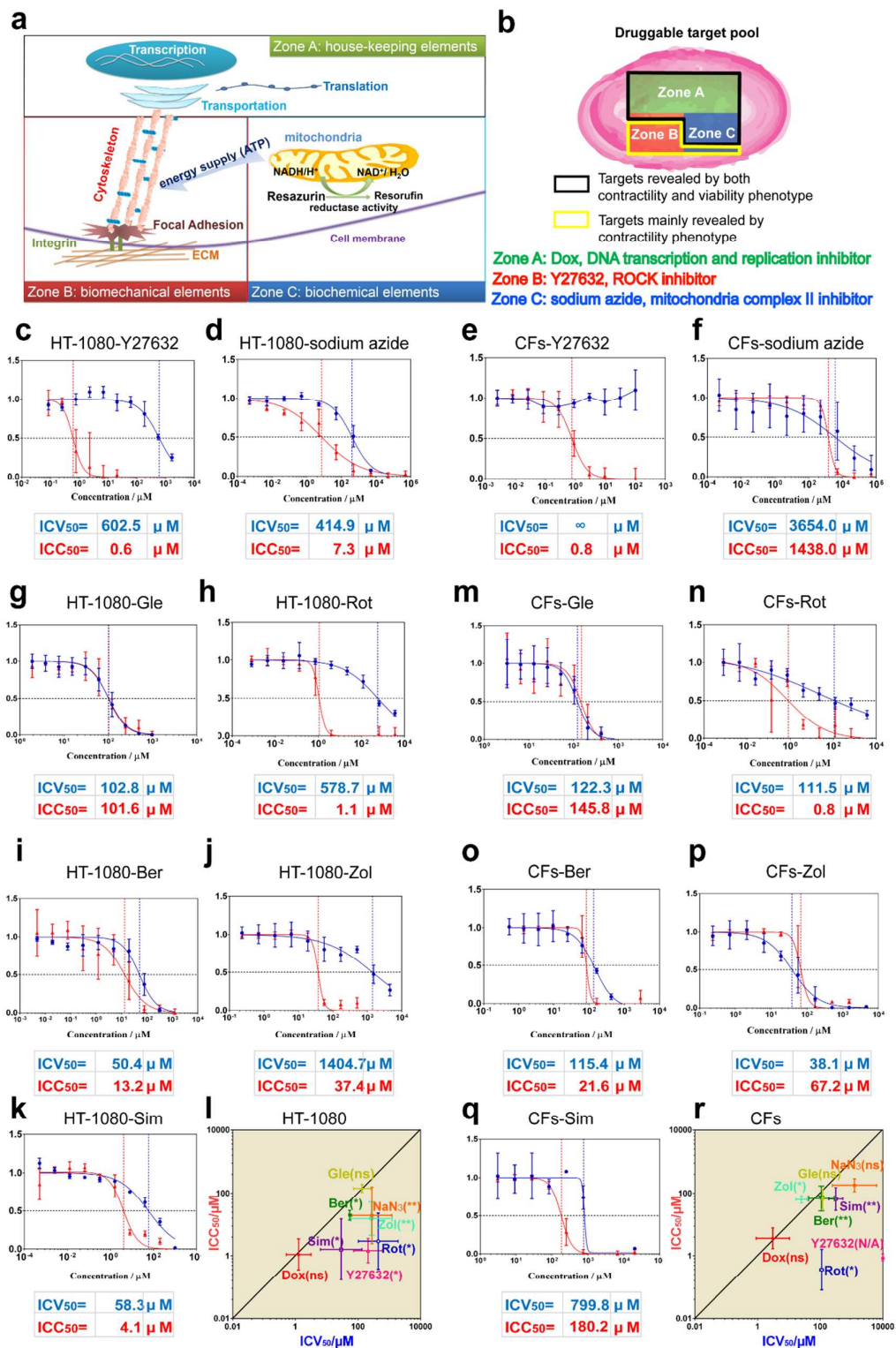


**Figure 4.** Revelation of novel MOAs by 3CChip. a) Schematic illustration of contractility phenotype-related molecular elements, which is categorized into house-keeping elements (Zone A), biomechanical elements (Zone B) and biochemical elements (Zone C). b) Experimental design to prove the running hypothesis of extended target pool enabled by 3CChip. c-f) Effects of Y27632 and sodium azide on contractility and viability of HT-1080 and

CFs as revealed by dose response curves ( $n \geq 3$ ). g-k) Dose response curves of five compounds against HT-1080 for combinatorial analysis of ICC and ICV. ( $n \geq 3$ ) l) Summary of ICC50 and ICV50 of the eight compounds against HT-1080. m-q) Dose response curves of five compounds against CFs for combinatorial analysis of ICC and ICV. r) Summary of ICC50 and ICV50 of the eight compounds against CFs. P value  $\geq 0.05$ : ns (not significant);  $0.01 < P$  value  $< 0.05$ : \*,  $0.001 < P$  value  $< 0.01$ : \*\*

regulatory networks of contractility. Up-stream house-keeping cellular functions in Zone A such as transcription and translation are postulated to influence both contractility phenotype and other phenotypes like cell viability. Zone B includes critical biomechanical elements for contractility regulation. As representative, integrin dependent focal adhesions dominate interaction between cells and matrix, linking the extracellular collagen fibrils to intercellular contractile filaments to form a robust intrinsic force network within the micro-tissue. Actin filaments interact with myosin motors, which move these filaments with respect to each other consuming energy from ATP hydrolysis, initiating the remodeling of collagen lattices. Drugs targeted to those biomechanical elements are expected to be faithfully revealed by contractility phenotype. Meanwhile, biochemical elements related to mitochondria activity in Zone C are also vital for regulation of cellular contractility as energy supply by mitochondria is required for ATP-dependent contraction. In contrast, resazurin reduction as underlying biochemistry of Alamar Blue assay is mostly relied on mitochondria activity.

Based on the above analysis of molecular-level working mechanism, we infer that contractility-based phenotypic readout would be more predictive to reveal drug effects than canonical cell viability readout when biomechanical elements are extensively involved along with biochemical elements. To verify this hypothesis, a cytoskeleton regulator Y-27632 [selectively inhibiting Rho-associated protein kinase (ROCK)] and the mitochondria toxin sodium azide (inducing chemical hypoxia) as well as Dox (intercalating DNA to stop replication and transcription) were examined for their ability to interrupt cellular contractility or Alamar Blue

reduction (Fig. 4b-f). Surprisingly, while Y-27632 practically showed little ( $ICV_{50}=602.5 \mu\text{M}$  for HT-1080) or even no ( $ICV_{50}=\infty$  for CFs) effect on cell viability, its inhibitory action on cellular contractility was evident ( $ICC_{50}=0.6 \mu\text{M}$  for HT-1080,  $ICC_{50}=0.8 \mu\text{M}$  for CFs). This result suggests that contractility-based phenotypic screening enlarged target pool, potentially leading to discovery of candidates with novel MOAs, which are otherwise undetectable with conventional phenotypic readouts. As for sodium azide treatment, contractility-based readout turned out to be more susceptible than viability as shown by the leftward shift of the ICC curve ( $ICC_{50}=7.3 \mu\text{M}$ ) relative to the ICV curve ( $ICV_{50}=414.9 \mu\text{M}$ ) for HT-1080. For CFs,  $ICC_{50}$  (1,438.0  $\mu\text{M}$ ) also decreased compared to  $ICV_{50}$  (3,654.0  $\mu\text{M}$ ). As comparison, cellular response to Zone A-targeted Dox showed similar trend in ICV and ICC curves for both HT-1080 and CFs (Fig. 3c,d). These results strongly indicate that contractility-based phenotypic screening could reveal drug interaction with potential targets in Zone B and Zone C with better sensitivity and prediction.

### 3.5. Evaluation and profiling of multiple drugs by 3CChip

To further reveal the characteristics of contractility-based drug assessment, five clinically available drugs [*i.e.* Gleevec (Gle), Rotenone (Rot), Zoledronate (Zol), Berberine (Ber) and Simvastatin (Sim)] were applied with concentration gradient to obtain combinatorial bi-content dose-response curves (Fig. 4g-k, m-q). Gle as a well-studied tyrosine kinase inhibitor<sup>23</sup> illustrated nondiscriminatory effects between contractility and viability for both cell types ( $ICC_{50}=101.6 \mu\text{M}$  for HT-1080 and 145.8  $\mu\text{M}$  for CFs;  $ICV_{50}=102.8 \mu\text{M}$  for HT-1080 and 122.3  $\mu\text{M}$  for CFs), which is not surprising given the broad participation of tyrosine kinase in cell signaling transductions. As for Rot, it was interesting to see that this well-known mitochondria toxin inhibited contractility more efficiently than viability ( $ICC_{50}=1.1 \mu\text{M}$  for HT-1080 and 0.8  $\mu\text{M}$  for CFs;  $ICV_{50}=578.7 \mu\text{M}$

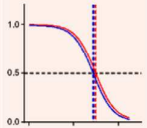
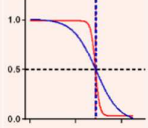
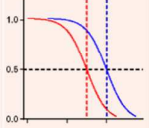
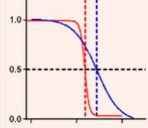
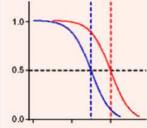
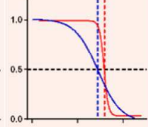
for HT-1080 and 111.5  $\mu\text{M}$  for CFs). This can be partially explained by the overlaps of energy supply between Zone B and Zone C. More importantly, apart from its functionality in inhibiting mitochondria complex I, Rot has also been proved to destabilize the cytoskeleton component microtubules.<sup>24</sup> As both inhibitory effects in Zone B and Zone C can be reflected by contractility, the ICC curve showed dramatic sensitivity of Rot response compared to ICV curve. Similar trend was observed in drug effects of Ber (ICC<sub>50</sub>=13.2  $\mu\text{M}$  for HT-1080 and 21.6  $\mu\text{M}$  for CFs; ICV<sub>50</sub>=50.4  $\mu\text{M}$  for HT-1080 and 115.4  $\mu\text{M}$  for CFs), which has been reported to exhibit anti-fibrotic effects in animal models.<sup>25, 26</sup> Bisphosphonate Zol has previously been thought to act primarily by blocking farnesyl diphosphate (FPP) formation in the isoprene biosynthesis pathway, with which biomechanical elements involving Rho and Rac signaling pathway (critical in biomechanical signals) were closely interacted.<sup>27</sup> Consistent with the proposed mechanism, ICC curve of Zol showed leftward shift relative to ICV curve for HT-1080, with approximately 40 folds decrease in ICC<sub>50</sub> (37.4  $\mu\text{M}$ ) compared to ICV<sub>50</sub> (1404.7  $\mu\text{M}$ ), indicating possibility to apply bisphosphonates in cancer therapies. However, it should be noted that the anti-contractility effect of Zol was no longer prominent in CFs (ICC<sub>50</sub>=67.2  $\mu\text{M}$ ; ICV<sub>50</sub>=38.1  $\mu\text{M}$ ). The difference might be owing to enhanced intrinsic contractility in  $\alpha$ -smooth muscle actin ( $\alpha$ -SMA) positive CFs, whereas HT-1080 was negative for  $\alpha$ -SMA expression (Supplementary Fig. 13). Sim, primarily used for treatment of dyslipidemia and prevention of cardiovascular disease, acts by inhibiting 3-hydroxy-3-methylglutaryl coenzyme A (HMG-CoA) reductase, which is responsible for the endogenous production of cholesterol.<sup>28</sup> The 3CChip experiment with Sim displayed dramatic enhancement of contractility inhibition as compared to cell viability for both HT-1080 and CFs (ICC<sub>50</sub>=4.1  $\mu\text{M}$  for HT-1080 and 180.2  $\mu\text{M}$  for CFs; ICV<sub>50</sub>=58.3  $\mu\text{M}$  for HT-1080 and 799.8  $\mu\text{M}$



for CFs). Since there was few study showing effects of Sim on cellular contractility especially in 3D,<sup>29</sup> we conducted further investigations into the MOAs of Sim in the following section.

As summary,  $ICV_{50}$  (lateral axis) and  $ICC_{50}$  (vertical axis) for all the nine compounds obtained above were plotted in one matrix for both HT-1080 and CFs (Fig. 4I,r). Theoretically, targets of drugs close to the diagonal path are profiled to Zone A, while those far apart from the diagonal path are expected to be profiled to Zone B or Zone C (Fig. 4a,b). Furthermore, cellular response curves obtained by 3CChip were categorized into three main types (Table 1) according to the relative magnitude of  $ICV_{50}$  and  $ICC_{50}$  (*i.e.* Type A:  $ICV_{50}=ICC_{50}$ ; Type B:  $ICV_{50}>ICC_{50}$ ; Type C:  $ICV_{50}<ICC_{50}$ ). For each category, the subset was further classified based on whether there were intersections between the two curves. Interestingly, we only observed intersected curve patterns in experiments performed with CFs, but not with HT-1080. The difference might be interpreted by stronger inherent contractility of CFs compared to HT-1080. Moreover, it is important to note that no curve pattern of Type C1 has been obtained in this study, but we do not rule out the possibility, which might be realized by specific inhibitor of resazurin reductase. So far, potential drug targets can be profiled to either Zone A or Zone B/C according to different types of curve patterns.

**Table 1.** Summary of ICC and ICV curve patterns.

Types	$ICV_{50}=ICC_{50}$		$ICV_{50}>ICC_{50}$		$ICV_{50}<ICC_{50}$	
Subtypes	Type A1	Type A2	Type B1	Type B2	Type C1	Type C2
Curve patterns						
Example	HT-1080-Dox	CFs-Dox	HT-1080-Y27632	CFs-Ber	–	CFs-Zol



### 3.6. MOAs profiling of sodium azide and Sim by 3CChip

Next, we asked how to distinguish drug effects on biomechanical elements from that on biochemical elements in an attempt of further profiling MOAs of drugs targeted to Zone B or Zone C. Based on the previous drug assessment results, Sim and sodium azide were selected for further studies on MOAs profiling and validation. TGF- $\beta$ 1 has been widely used as epithelial to mesenchymal transition (EMT) promoting factor that could stimulate contractility,<sup>30, 31</sup> and glucose level in medium is closely related to mitochondrial respiration.<sup>32</sup> Based on these prior knowledge, we hypothesize that involvement of TGF- $\beta$ 1 (stimulator of contractility) and glucose (stimulator of viability) in 3CChip will facilitate preliminary profiling of drug MOAs (Fig. 5a). Briefly, involvement of biomechanical regulator TGF- $\beta$ 1 is supposed to cause shift of ICC curve, while involvement of biochemical regulator glucose is supposed to cause shift of both ICC and ICV curve. To obtain a quantitative index for curve shift, ratio between ICV<sub>50</sub> and ICC<sub>50</sub> is defined as pseudo Therapeutic Index (pTI), which is referred to the well-known term of Therapeutic Index (TI) used in pharmacology (defined as the ratio of lethal dose to effective dose at 50% populations, see Methods). When the biochemical elements in Zone C is blocked by the mitochondria activity inhibitor sodium azide, glucose alteration no longer gave rise to change of pTI (Figure 5b,c, upper right). Instead, addition of TGF- $\beta$ 1 during sodium azide exposure resulted in transforming of the two curves with significantly decreased pTI (Figure 5b,c, upper left). These results indicate the reliability of this method for preliminary profiling of drug MOAs. Similar sets of experiments were then performed with Sim and an opposite trend to sodium azide was observed. Addition of TGF- $\beta$ 1 during Sim exposure did not change the pTI values (Figure 5b,c, lower left), while variation of glucose levels evidently altered the pTI values. (Figure 5b,c, lower right). This is

consistent with previous suspicion that Sim can block biomechanical elements in Zone B.

Molecular investigations on biomechanical elements in Zone B were performed to further confirm profiled MOAs of Sim. Since molecular mechanism of sodium azide has been previously well studied, it was used as control together with solvent DMSO. We began by performing traditional Live/Dead staining to visually detect cell morphology and cell membrane integrity (Fig. 5d). While keeping 'alive', both HT-1080 and CFs exposed to Sim did not spread and showed rounded morphology with PI signal barely detected. As the most important component of cytoskeleton, loss of F-actin caused by Sim administration (Fig. 5e) immediately restrained contraction phenotype. Moreover, in agreement with previous studies in 2D,<sup>29</sup> focal adhesion (elements in Zone B) illustrated by clustering of vinculin and paxillin, was obviously disrupted by Sim in CFs (Fig. 6f). We also observed down regulation of vinculin and paxillin by Sim in HT-1080, yet they did not cluster but diffusely distributed throughout the cytoplasm.<sup>33</sup> In contrast, sodium azide at the concentration of  $IC_{50}$  did not alter all the above biomechanical elements, as revealed by equivalent expression and assembling of cytoskeleton and focal adhesion complex compared to the solvent treated group. These results suggest that Sim targeted signal networks were closely related to biomechanical elements in Zone B, implying possibility of using Sim to treat disease such as fibrosis or tumour metastasis. Although great promise of target profiling by 3CChip has been proved here, we must make it clear that the profiling capacity is still quite limited in terms of accuracy and resolution. Nevertheless, there is no doubt that the simple-to-use and cost-effective 3CChip provides additional information and better prediction for drug target deconvolution.

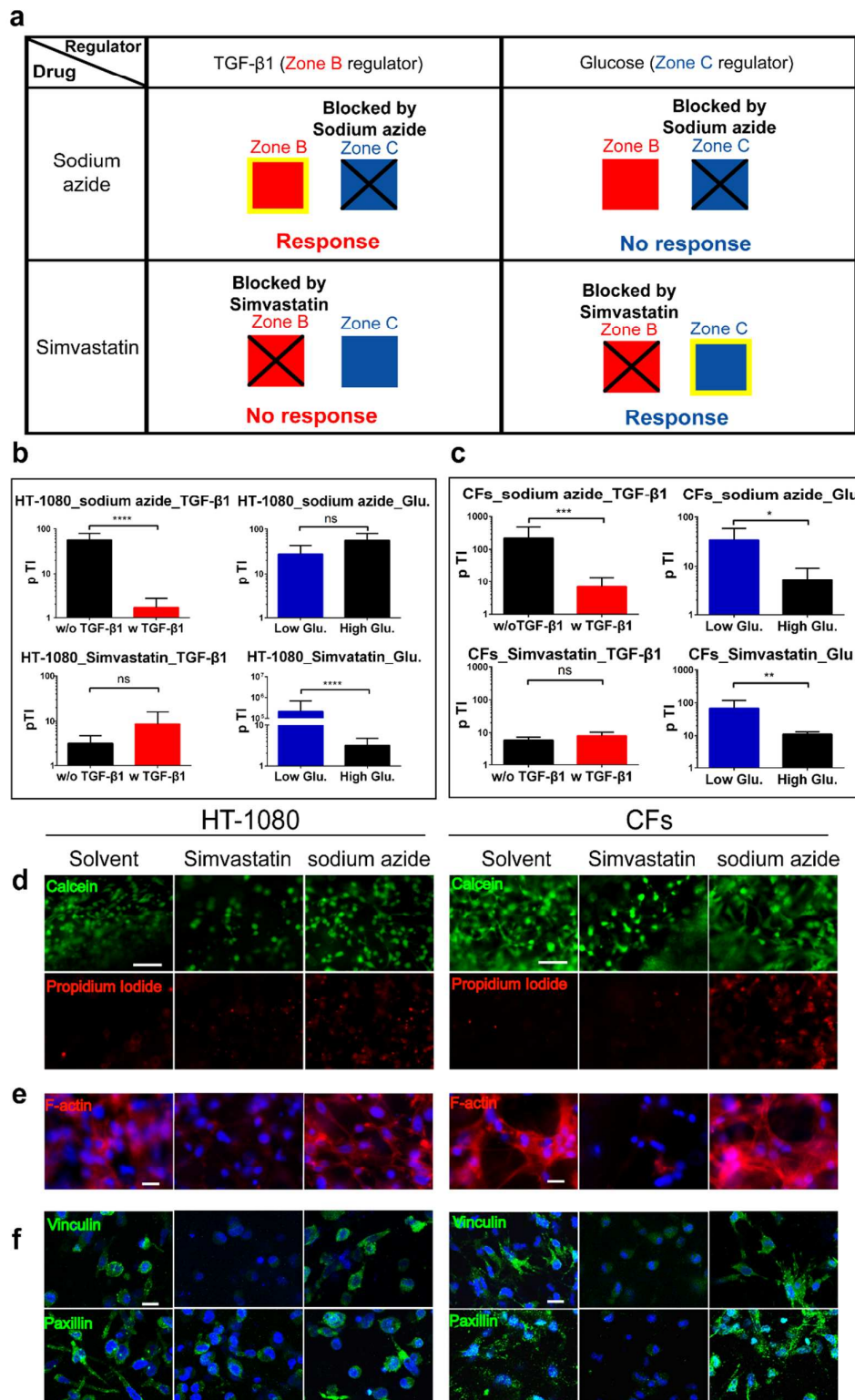


**Figure 5.** Profiling and validation of MOAs of sodium azide and Simvastatin by 3CChip. a) Schematic demonstration of TGF- $\beta$ 1 and glucose involvement for MOAs profiling of sodium azide and Simvastatin. b, c) Effects of biomechanical elements-regulator TGF- $\beta$ 1 and biochemical elements-regulator glucose on dose

response curves of drugs (Simvastatin or sodium azide). (b) for HT-1080, (c) for CFs. A parameter, pTI (pseudo Therapeutic Index, the ratio of ICV50 and ICC50) is defined to indicate the potency of a drug under a particular condition. (n=6). d) Calcein AM (Green) and PI (Red) staining of HT-1080 and CFs treated by solvent, Simvastatin and sodium azide, respectively. Scale bar: 100  $\mu\text{m}$ . e) F-actin (Red) staining of HT-1080 and CFs treated by solvent, Simvastatin and sodium azide, respectively. Scale bar: 25  $\mu\text{m}$ . f) Immunofluorescence staining of focal adhesion (Green: vinculin or paxillin; Blue: Hoechst) in HT-1080 and CFs treated by solvent, Simvastatin and sodium azide, respectively. Scale bar: 20  $\mu\text{m}$ . Data are shown as mean $\pm$ SD. Symbols for statistical significance: P value $\geq$ 0.05: ns (not significant); 0.01<P value<0.05: \*, 0.001<P value<0.01: \*\*; 0.0001<P value<0.001: \*\*\*, P value<0.0001: \*\*\*\*.

#### 4. Discussion

The goal of this study is to develop innovative phenotypes for discovering new druggable MOAs. One of the advancements of the 3CChip is the expanded MOAs pool, evidenced by the dramatic inhibition effects of Y23672 on contractility, regardless of less to no alteration in viability. We anticipate this advancement will accelerate clinical relevant drug discoveries that contribute to novel therapeutic strategies. For instance, proliferation inhibition has been the dominant theme in cancer drug discovery for decades, while targeting cell migration is proposed as promising alternative to control cancer cell metastasis. Signaling mediators fall into Zone B (biomechanical elements, *e.g.* adhesive complex, cytoskeleton elements) are closely coincident with that of cell migration. Therefore, it is reasonable to predict that the contractility inhibitory compounds might be potential anti-metastatic drug candidates.

As a routine experimental artifice for fibroblast relevant investigation, collagen contraction assay is conventionally performed in large-scale based on multi-well plate (*e.g.* 6-well plate, 24-well plate), which is accompanied by high cost (expensive commercialized collagen solutions and a large number of cell consumption) and complicated operation procedures from cell seeding to gel area measurement. A paucity of studies has shown the effort to fabricate miniaturized collagen gels. Pioneering works done by Christopher S. Chen's group opened up avenues to generate collagen gel based micro-tissues using soft lithography techniques.<sup>34, 35</sup> Guan et al.

recently reported the development of micro-collagen gel array ( $\mu$ CGA) using micro-well PDMS devices for long-term single-cell 3D culture and heterogeneity analysis of cell proliferation.<sup>36</sup> Aqueous two-phase system has also been used to produce dextran-rich micro-scale collagen gels in PEG-rich medium with the ultimate goal to improve mass transfer in 3D cell culture format.<sup>20</sup> Despite of these improvements in collagen gel based 3D assays, no study showed the possibility to utilize cellular contractility for high throughput phenotypic drug screenings, which is the core of 3CChip demonstrated in the current study. The facile and rapid on-chip generation of collagen-based micro-tissues is applicable for other types of biomaterials (*e.g.* matrigel, alginate and PEG) and the isolated reaction unit also allows other bio-assays (*e.g.* immunofluorescence staining) to be conducted on the chip.

Although cellular contractility dominates collagen contraction rate, the gel area can also be affected by other parameters such as cell density and collagen gel concentration. Therefore, optimization of these conditions is recommended for a particular disease model to obtain expected contraction without drug engagement. Another important, yet not systematically studied, issue for this platform is the time course of contraction, which is non-linear. Most of classical phenotypic assays, including Alamar Blue assay used here, are limited to only reflect the end-point stage of the interested samples. The endpoint readout only provides snapshot to demonstrate the accumulative molecular or cellular response after long-term drug treatment. In contrast, the dynamic gel contraction phenotype likely opens up with new possibility to record the entire process of micro-tissue transformation upon drug administration. As supported by our preliminary experimental analysis (Supplementary Fig. 14), data collected at diverse time points after drug loading exhibited different patterns of corresponding ICC and ICV curves. We deem time effects

as a double-bladed sword, as for one side, time-dependent shift of curves is potentially informative for further deduction of drug MOAs, while in another aspect, great caution is required to determine which time point should be selected. Future works will explore the utility and mechanism of 3CChip for dynamic analysis based on time-lapse imaging and also a collective data pool comprised of more disease models and drugs.

The challenge for conventional 'black-box' phenotypic drug discovery is to seek out potential targets hit by the drug candidate after a disease-modifying phenotype is observed. Mechanism-informed phenotypic screenings with detailed and unbiased multi-parametric features show great power to determine the degree of similarity of MOAs of different compounds and will considerably aid target deconvolution.<sup>2</sup> It is important to note that the target profiling enabled by the 3CChip is currently limited in being able to roughly classifying the targets into three broad categories. The identified category will then allow the development of a small, but highly relevant array of reporters for drug screening readouts. TGF- $\beta$ 1 and glucose were applied to the 3CChip contributing to discrimination between the biomechanical and biochemical effects. We believe that further improvement of predictability for target profiling could be achieved by introducing more detailed and systematical methodologies such as bioinformatics analysis on comprehensive pathways crosstalk.

The first-version of 3CChip reported in this study is not designed as an exact re-creation of the *in vivo* diseased tissues (*i.e.* tumor or fibrotic tissues). Future involvement of various cell types and designs mimicking their physio/pathological features will be considered to obtain more biomimetic and relevant results. For example, involvement of cardiomyocytes in the cardiac fibrosis model may provide additional information on drug induced myocardial toxicity. The

bi-content 3CChip can be further incorporated with other phenotypic readouts (*e.g.* ATP release, gene reporter) to realize multi-content readouts,<sup>37</sup> which will offer greater opportunities to perform large-scale quantitative assays and greatly expand targets that can be explored.

## 5. Conclusions

Although molecular mechanism for inherent cellular contractility has been the research focus of cell biology for decades,<sup>21, 22</sup> there is still no study that linked cell contraction ability to phenotypic drug screenings. In the present work, we develop the 3CChip as a robust platform to translate cellular contractility as biomechanics-related readout for phenotypic drug assessment for the first time, which is operated in a high throughput, three-dimensional, label-free and cost-effective format. As a proof-of-concept study, the fibrosarcoma cell line HT-1080 comprising tumor model is investigated in parallel to primary CFs comprising cardiac fibrosis model. Bi-content analysis on ICC and ICV of the same sample is achieved by gel area calculation (imaged by iPhone and analyzed by homemade software) and Alamar Blue measurement respectively. As a result, for certain drugs and cells  $ICC_{50}$  equals to  $ICV_{50}$ , while in other cases the two parameters are quite distinguishable. Molecular investigation on cellular response upon drug administration reveals that drug screening performed on 3CChip might facilitate discovery of extended drug hits, in particular targets involved in cytoskeleton, cell adhesion or cell migration, which are difficult to be detected by traditional cell viability assays. Further analysis on relative positions of ICC and ICV curves opens up the possibility of primary target profiling that might contribute to target deconvolution. Owing to its simplicity and flexibility, we envision that the biomechanical phenotype based 3CChip will excite great interest in the context of preclinical pharmaceutical research and synergize with the rapid growing field of pharmacogenomics.

## Acknowledgements

This work was funded by the Natural Science Foundation of China (Grants 81171474, 51273106 and 51461165302), the Beijing Municipal Natural Science Foundation (Grant 157142090).

## References

1. W. Zheng, N. Thorne and J. C. McKew, *Drug discovery today*, 2013, **18**, 1067-1073.
2. J. G. Moffat, J. Rudolph and D. Bailey, *Nature reviews. Drug discovery*, 2014, **13**, 588-602.
3. S. N. Rampersad, *Sensors*, 2012, **12**, 12347-12360.
4. B. B. Aggarwal, G. Sethi, V. Baladandayuthapani, S. Krishnan and S. Shishodia, *Journal of cellular biochemistry*, 2007, **102**, 580-592.
5. F. C. Ramaekers and F. T. Bosman, *The Journal of pathology*, 2004, **204**, 351-354.
6. J. Friedrich, C. Seidel, R. Ebner and L. A. Kunz-Schughart, *Nature protocols*, 2009, **4**, 309-324.
7. C. Fischbach, R. Chen, T. Matsumoto, T. Schmelzle, J. S. Brugge, P. J. Polverini and D. J. Mooney, *Nature methods*, 2007, **4**, 855-860.
8. L. A. Gurski, A. K. Jha, C. Zhang, X. Jia and M. C. Farach-Carson, *Biomaterials*, 2009, **30**, 6076-6085.
9. K. H. Nam, A. S. Smith, S. Lone, S. Kwon and D. H. Kim, *Journal of laboratory automation*, 2014, DOI: 10.1177/2211068214557813.
10. W. Liu, Y. Li, S. Feng, J. Ning, J. Wang, M. Gou, H. Chen, F. Xu and Y. Du, *Lab on a chip*, 2014, **14**, 2614-2625.
11. C. J. Lovitt, T. B. Shelper and V. M. Avery, *Assay and drug development technologies*, 2013, **11**, 435-448.
12. E. Bell, B. Ivarsson and C. Merrill, *Proc. Natl. Acad. Sci. USA*, 1979, **76**, 1274-1278.
13. F. Grinnell, C. H. Ho, Y. C. Lin and G. Skuta, *Journal of Biological Chemistry*, 1999, **274**, 918-923.
14. J. T. Parsons, A. R. Horwitz and M. A. Schwartz, *Nature reviews. Molecular cell biology*, 2010, **11**, 633-643.
15. X. Li, X. Zhang, S. Zhao, J. Wang, G. Liu and Y. Du, *Lab on a chip*, 2014, **14**, 471-481.
16. H. Zhao, X. Li, S. Zhao, Y. Zeng, L. Zhao, H. Ding, W. Sun and Y. Du, *Biofabrication*, 2014, **6**, 045009.
17. A. Ozcan, *Lab on a chip*, 2014, **14**, 3187-3194.
18. X. D. Liu, M. Skold, T. Umino, Y. K. Zhu, D. J. Romberger, J. R. Spurzem and S. I. Rennard, *The Journal of laboratory and clinical medicine*, 2000, **136**, 100-109.
19. D. M. Gilkes, L. Xiang, S. J. Lee, P. Chaturvedi, M. E. Hubbi, D. Wirtz and G. L. Semenza, *Proceedings of the National Academy of Sciences of the United States of America*, 2014, **111**, E384-393.
20. C. Moraes, A. B. Simon, A. J. Putnam and S. Takayama, *Biomaterials*, 2013, **34**, 9623-9631.
21. R. Levayer and T. Lecuit, *Trends in cell biology*, 2012, **22**, 61-81.
22. K. Burrige, K. Fath, T. Kelly, G. Nuckolls and C. Turner, *Annual review of cell biology*, 1988, **4**, 487-525.
23. P. Vigneri and J. Y. Wang, *Nature medicine*, 2001, **7**, 228-234.



24. A. J. Wolpaw, K. Shimada, R. Skouta, M. E. Welsch, U. D. Akavia, D. Pe'er, F. Shaik, J. C. Bulinski and B. R. Stockwell, *Proceedings of the National Academy of Sciences of the United States of America*, 2011, **108**, E771-780.
25. P. Chitra, G. Saiprasad, R. Manikandan and G. Sudhandiran, *Toxicology letters*, 2013, **219**, 178-193.
26. B. J. Zhang, D. Xu, Y. Guo, J. Ping, L. B. Chen and H. Wang, *Clinical and experimental pharmacology & physiology*, 2008, **35**, 303-309.
27. Y. Zhang, R. Cao, F. Yin, F. Y. Lin, H. Wang, K. Krysiak, J. H. No, D. Mukkamala, K. Houlihan, J. Li, C. T. Morita and E. Oldfield, *Angewandte Chemie*, 2010, **49**, 1136-1138.
28. J. K. Liao and U. Laufs, *Annual Review of Pharmacology and Toxicology*, 2005, **45**, 89-118.
29. M. Copaja, D. Venegas, P. Aranguiz, J. Canales, R. Vivar, Y. Avalos, L. Garcia, M. Chiong, I. Olmedo, M. Catalan, L. Leyton, S. Lavandero and G. Diaz-Araya, *Toxicology*, 2012, **294**, 42-49.
30. M. R. Weist, M. S. Wellington, J. E. Bermudez, T. Y. Kostrominova, C. L. Mendias, E. M. Arruda and L. M. Larkin, *Journal of tissue engineering and regenerative medicine*, 2013, **7**, 562-571.
31. P. Lijnen, V. Petrov, K. Rumilla and R. Fagard, *Methods and findings in experimental and clinical pharmacology*, 2003, **25**, 79-86.
32. V. M. Gohil, S. A. Sheth, R. Nilsson, A. P. Wojtovich, J. H. Lee, F. Perocchi, W. Chen, C. B. Clish, C. Ayata, P. S. Brookes and V. K. Mootha, *Nature biotechnology*, 2010, **28**, 249-255.
33. S. I. Fraley, Y. Feng, R. Krishnamurthy, D. H. Kim, A. Celedon, G. D. Longmore and D. Wirtz, *Nature cell biology*, 2010, **12**, 598-604.
34. T. Boudou, W. R. Legant, A. Mu, M. A. Borochin, N. Thavandiran, M. Radisic, P. W. Zandstra, J. A. Epstein, K. B. Margulies and C. S. Chen, *Tissue engineering. Part A*, 2012, **18**, 910-919.
35. R. Zhao, C. S. Chen and D. H. Reich, *Biomaterials*, 2014, **35**, 5056-5064.
36. Z. Guan, S. Jia, Z. Zhu, M. Zhang and C. J. Yang, *Analytical chemistry*, 2014, **86**, 2789-2797.
37. X. Yan, J. Wang, L. Zhu, J. J. Lowrey, Y. Zhang, W. Hou, J. Dong and Y. Du, *Lab on a chip*, 2015, DOI: 10.1039/c5lc00313j.